Supplemental Methods

Cytospin for cytology

50.10^3 differentiated cells from D6 to D20 were cytospun (Cytospin3, Shandon) onto glass slides (Matsunami). Cytological analysis was performed after May-Grünwald Giemsa (MGG) staining (Sigma) according to manufacturer's instruction.

Immunoblots

Cells were harvested at one million per ml per condition, washed in 1X PBS and lysed on ice in RIPA buffer (Sigma) containing protease and phosphatase inhibitors cocktail (Thermofisher). Lysates were gently sonicated, centrifuged and protein concentration was quantified using Bradford assay (Interchim). After standard procedures of SDS-polyacrylamide gel electrophoresis, nitrocellulose membrane transfer and 5% non-fat milk blocking, blotting was performed using 1/1000 diluted primary antibodies (references in **Suppl. Table 3**). Bound primary antibodies were detected using anti-mouse (Sigma) or anti-rabbit (Thermofisher) horseradish peroxidase- conjugated secondary antibody. Revelation was performed by enhanced chemiluminescent substrate (Thermofisher) and signals were visualized using Chemidoc Device (BioRad).

RQ-PCR

Total RNA from fresh cells was isolated, treated with DNAse I, using the RNeasy Mini Kit from Qiagen. RNA quantity was determined with the NanoDrop ND-1000 Spectrophotometer (Thermo Fisher Scientific). For each sample, 500 ng of RNA was subjected for reverse transcription reaction (Reverse Transcription Kit, Thermofisher). Expression levels of GPX4 and GAPDH were measured by real time PCR using Taqman probes (Thermofisher). For the gene expression ratios of GPX1 versus GAPDH housekeeping gene, real time PCR was performed by power SYBR green assay (Thermofisher). Primer sequences are listed **Suppl. Table 4**. Experiments were realized in the Quant Studio 7 Detection Device (Applied Biosystems), including dissociation curves setting. The comparative C_T method was used for quantification of gene expression.

Imaging Flow Cytometry (IFC)

Enucleation was evaluated in Day18 erythroblasts cells on ImageStream®^{X} Mark II (Amnis/Luminex) using INPIRE™ software (200.1.388.0). 1.10^6 cells in 50µl 1X PBS were

stained with human Anti-GPA_PE, AlexaFluor 488-conjugated Anti Phospho Myosin Light Chain, AlexaFluor 647-conjugated Cholera Toxin subunit b and Hoechst or DRAQ7. Cell analyses were performed on at least 10,000 cells at 60X magnification. Analysis was performed using IDEAS™ software (6.2.64.0). First, saturated, clipped and not focused events were gated out. Then, erythroblasts, reticulocytes and pyrenocytes were identified thanks to Hoechst and GPA stainings. Erythroblasts enucleation was evaluated on 'Delta Centroid XY_M03_CD235_PE_IntensityWeighted_M01_Hoechst' vs 'Aspect Ratio_M04'. The precise gating strategy is explained **Suppl. Fig 6**. The graphical definitions of the gating strategy used to evaluate precisely the enucleation process are detailed below:

Focused = graphical region on All
NonSat[xx] = graphical region on All, for each xx collected channel
Uncut = graphical region on All
DNA+ = graphical region on Events
SingleNucleus = graphical region on DNA+
CD235+_for Ery = graphical region on Mono-Nucleated
CD235+_for Ret = graphical region on DNA-
SingleRet = graphical region on CD235+_for Ret
Pyr = graphical region on Mono-Nucleated
Ery = graphical region on Mono-Nucleated

Combined populations:
Events = NoSat&Uncut&Focused
DNA- = Events And Not DNA+ & Events
MonoNucleated = SingleNucleus & DNA+ & Events
Erythroblasts = CD235+_forEry & Mono-Nucleated And Ery
Reticulocytes = SingleRet & CD235+_forRet & DNA-
Pyrenocytes = Pyr & Mono-Nucleated

Neutral lipid quantification

For each condition, 10^6 cells were frozen at -80°C then sent to MetaToul Lipidomique Core Facility (Toulouse, France). Samples were homogenized, extracted with ISTD by the Bligh and Dyer method, final extracts were solubilized in 20μL ethyl acetate and analyzed by gas chromatography with flame-ionization detection (Focus Finningan, Thermo Scientific) using

Zebron ZB-5ms column (Phenomenex). Quantification was relative using internal calibration (Stigmasterol, Cholesterol ester C17, TG 19).

Suppl. table 1: Sequences of the 3 GPX4 ShRNA

SIGMA Sh Rna Collection-TRC		Sh sequences	Validated
TRCN0000046249	SH1	CCGG*GTGAGGCAAGACCGAAGTAAACTC***GAGTTTACTTCGGTCTTGCCTCAC**TTTTTG	*Cell.2014. Stockwell and al.*
TRCN0000304065	SH2	CCGG*TCATGACGGCCTGCCTGCAAACTC***GAGTTTGCAGGCAGGCCGTCATG**ATTTTTG	
TRCN0000046251	SH3	CCGG*GTGGATGAAGATCCAACCCAACTC***GAGTTGGGTTGGATCTTCATCCAC**TTTTTG	

Suppl. table 2: List of antibodies used for FCM

D1 to D6	D7 to D14	D14 to D20	D16 to D20
CD34PE (AC136) CD36Vioblue (REA760) CD71FITC (REA902) CD235aAPC (REA175)	CD71PE CD235APC	CD71FITC or BAND3FITC* (BRIC6) CD235PE CD49dAPC (REA545)	HOECHST, CD71FITC or BAND3FITC*, CD235APC

All conjugated antibodies and corresponding isotypes were supplied from Miltenyi Biotec, excepted *BAND3 FITC purchased from IGBRL. Hoechst was supplied from Sigma.

Suppl. table 3: List of antibodies used for immunoblots

Antibodies Targets	Antibodies species	References
Anti-human GPX4	rabbit	Abcam (25066)
Anti-human GPX1	rabbit	Thermofisher (PA5-26323)
Anti-human Phospho Myosin Light Chain	mouse	Cell signaling (3675)
Anti-human Myosin Light Chain	rabbit	Cell signaling (8505)
Anti-human Catalase	mouse	Santacruz (271242)
Anti-human GAPDH	mouse	Santacruz (32233)

Suppl.table 4: List of primers for RQ-PCR

GPX4 and GAPDH primer pairs were designed to span an exon–exon boundary using Primer Blast tool, purchased by Eurogentec and validated for their specificity.

5'->3'

GPX4 FOR GCCTTTGCCGCCTACTGAA	*GPX4 REV* TCCTTGGCGGAAAACTCGTG
GAPDH FOR AAGGTGAAGGTCGGAGTCAA	*GAPDH REV* CTTGACGGTGCCATGGAATT

Legends to supplemental figures

Supplemental figure 1

A. Histogram showing *GPX4* gene expression at RNA level at different steps of *in vitro* erythropoiesis from Day2 (D2) to D17 (n=3).

B. Left: representative GPX4 immunoblot at different erythroid stages. GAPDH was used as internal control. Right: immunoblot quantification of the GPX4/GAPDH ratio from two independent experiments.

C. Left: representative GPX4 immunoblot, at D14 obtained from DMSO and 1μM RSL3-treated erythroblasts. GPX1 Western Blot was also performed and showed no difference between the two conditions. Right: quantification of the GPX4/GAPDH ratio from three independent experiments. DMSO *vs.* RSL3, p=.01

D. Left: representative GPX4 immunoblot, at D18, obtained from DMSO and 1μM RSL3-treated erythroblasts. Right: quantification from three independent experiments. DMSO *vs.* RSL3, p<.05.

*$p < 0.05$; **$p < 0.001$; ***$p < 0.0001$. Error bars are SEM.

Supplemental figure 2

A. Dot plots from a representative *in vitro* differentiation using our protocol, showing the loss of CD34, gain of CD36 from D0 to D5, the gain of GPA and progressive decrease in CD71 expression from D7 to D15 and the enucleation step at D18 with a population of $GPA^{High}/Band3^{+}/Hoechst^{-}$ (reticulocytes) or $GPA^{High}/Band3^{+}/Hoechst^{+}$ (OrthoE) cells and a population of $GPA^{Int}/Hoechst^{+}/Band3^{Low}$ cells (pyrenocytes).

B. IFC quantification of orthoE and enucleated $GPA^{+}/Hoechst^{-}$ reticulocytes after 1μMRSL3 or DMSO treatments (n=5). Gating strategy is shown in Suppl. Fig 6. Percent of enucleated cells DMSO *vs.* RSL3: 71 ±8% *vs.* 38 ±10%, p<.01.

Supplemental figure 3

A. Histogram showing *GPX4* gene expression at RNA level, using *GAPDH* as internal control, after lentiviral transduction of erythroblasts with scramble (SCR) shRNA as a control and 3 different GPX4-specific shRNA: SH1, SH2 and SH3 (n=3). *GPX4/GAPDH* ratio at RNA level were 0.35 ±0.03, 0.75 ±0.03 and 0.37 ±0.04 for SH1, SH2 and SH3 respectively. DMSO *vs.* SH1: p<.0001, *vs.* SH2: p<.001, *vs.*SH3: p<.0001.

B. Left: Histogram showing GPX4 expression at protein level, using GAPDH as internal control, after lentiviral transduction as described above (n=3). GPX4/GAPDH ratio were 0.22 ±0.02, 0.42 ±0.03 and 0.20 ±0.04 for SH1, SH2 and SH3 respectively. DMSO *vs.* SH1: p<.0001, *vs.* SH2: p<.0001, *vs.*SH3: p<.0001. Right: Representative GPX4 immunoblot from one of the three independent experiments.

C. GPX4 knockdown did not impact erythroid differentiation until OrthoE stage: dot plots are obtained from one representative experiment showing a similar expression pattern of erythroid markers at D5, D9 and D18 between shSCR and shGPX4-transduced cells (the figure shows data obtained with SH1 as an example) (n=3).

Supplemental figure 4

A. Sensitivity of three different cell lines after 12h RSL3 exposure in terms of lipid peroxidation assessed by C11-BODIPY$^{581/591}$staining. UT7-cells expressed low level of C11-BODIPY$^{581/591}$ (19.5 ±2%) in comparison to the U937 myeloid cells (38 ±2%) and the lymphoid cells RAMOS (52 ±3%) despite a 10-fold higher dose (1μM *vs.* 0.1μM).

B. Ferroptosis-indirect inducer, Erastin, did not impact enucleation at D20 (n=3). Percent of enucleated D20 cells: 71 ±6% *vs.* 67 ±6%, p= *NS*.

Supplemental figure 5

A. Scheme illustrating the crosstalk between cholesterol synthesis and GPX4 translation in cells. Isopentenyl pyrophosphate (IPP) is an intermediary component of the mevalonate pathway and is also necessary for Isopentenyl SEC-tRNA synthesis and translation of selenoproteins such as GPX4.

B. D20 erythroblast enucleation was significantly reduced after cell exposure to 2μM Simvastatin, an inhibitor of HMG-CoA reductase (n=3). Percent of enucleated cells DMSO *vs.* Simvastatin: 67 ±4 *vs.* 38 ±5%, p<.001

Supplemental figure 6

A. Schematic representation of the gating strategy for enuceation study by imaging flow cytometry. The different gates were defined to (i) identify pyrenocytes (Pyr), reticulocytes (Ret) and erythroblasts based on GPA (CD235)-PE and Hoechst staining (upper) and (ii) within the erythroblast gate, to identify successive steps in nucleus polarization (Init) and nucleus extrusion (Enuc 1,2,3, this latter corresponding to nearly completed enucleation) based on “deltacentroid in GPA^{+}/Hoechst^{+} cells *vs.* aspect ratio brightfield” dot plots (lower).

B. Representative images obtained from another experiment using DRAQ7 as nuclear staining and GPA, showing the progressive extrusion of the nuclei during the progression all along these defined gates, Enuc3 corresponding to the end of the enucleation process.

Supplemental figure 7

Representative immunofluorescence image of DMSO and RSL3-treated cells using Tubulin and CTB in association with DAPI, showing a strong CTB localization at cleavage furrow in DMSO-treated cells while the staining was more diffuse and weaker in 1µM RSL3-treated cells.

Supplemental figure 8

A. Representative images obtained with IFC using DRAQ7 (for nucleus staining), GPA (for membrane staining) and pMRLC between DMSO and 1µM RSL3 treated cells (n=1). The pMRLC fluorescence intensity was decreased in RSL3 condition in comparison to DMSO, confirming the data obtained by FCM and immunoblot.

B. Dot plots obtained from IFC in the Init and Enuc1 gates showing:

- Right: an identical GPA intensity in DMSO (black dots) and 1µM RSL3-treated (red dots)-cells (Y-axis), but a decreased total pMRLC signal intensity (X-axis)
- Left: an identical mean intensity on the Y-axis between these two conditions. The Y-axis corresponds to the concentration ratio of pMRLC at the interface between the nucleus and the cytoplasm",*i.e* the relative proportion of the total pMRLC signal located at a mask defined as the nucleus-cytoplasm junction.

Suppl. Figure 1

A

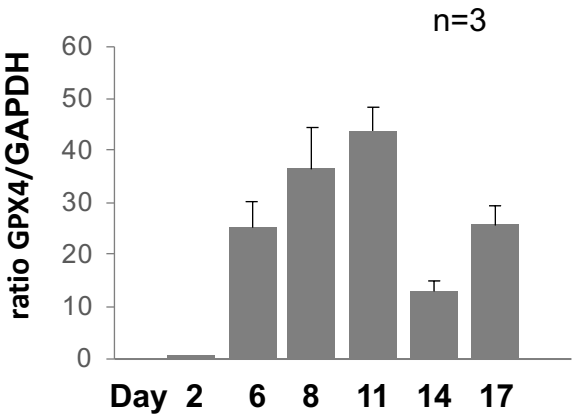

B

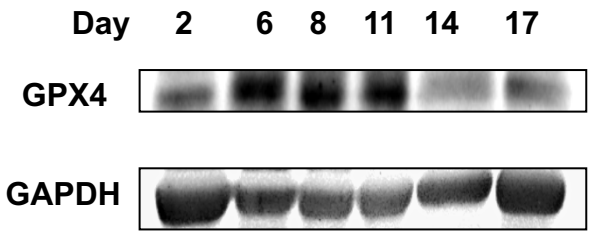

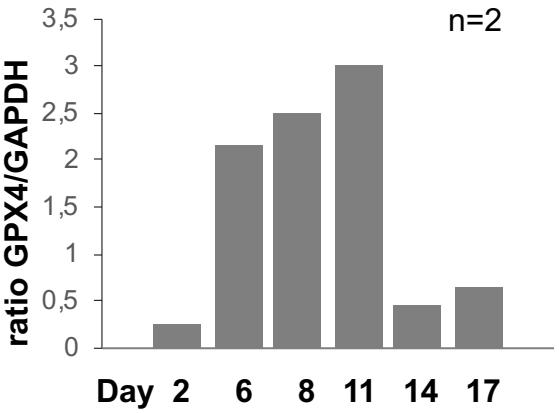

C

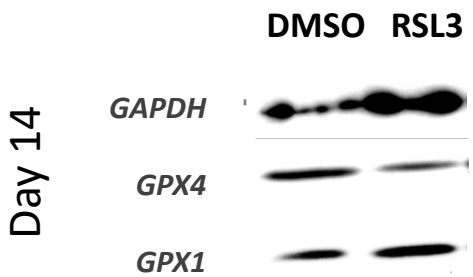

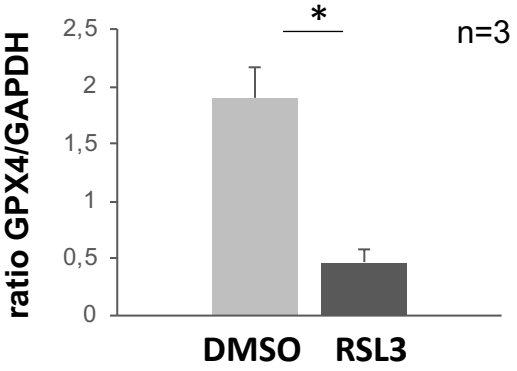

D

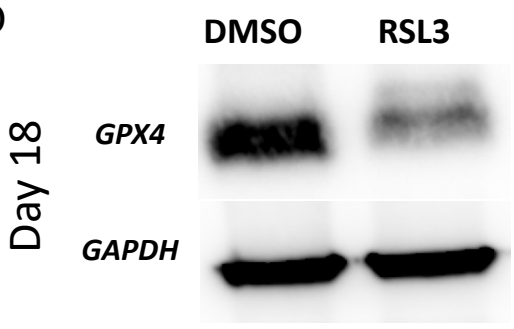

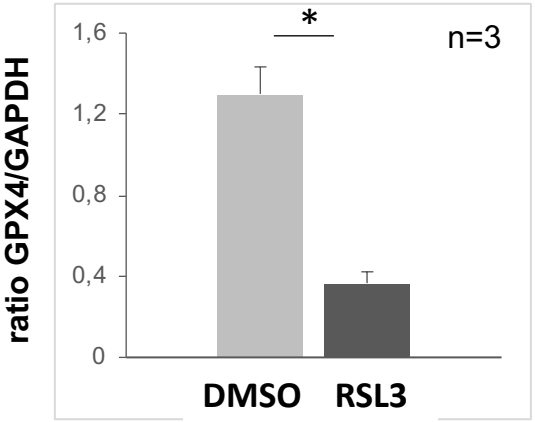

Suppl. Figure 2

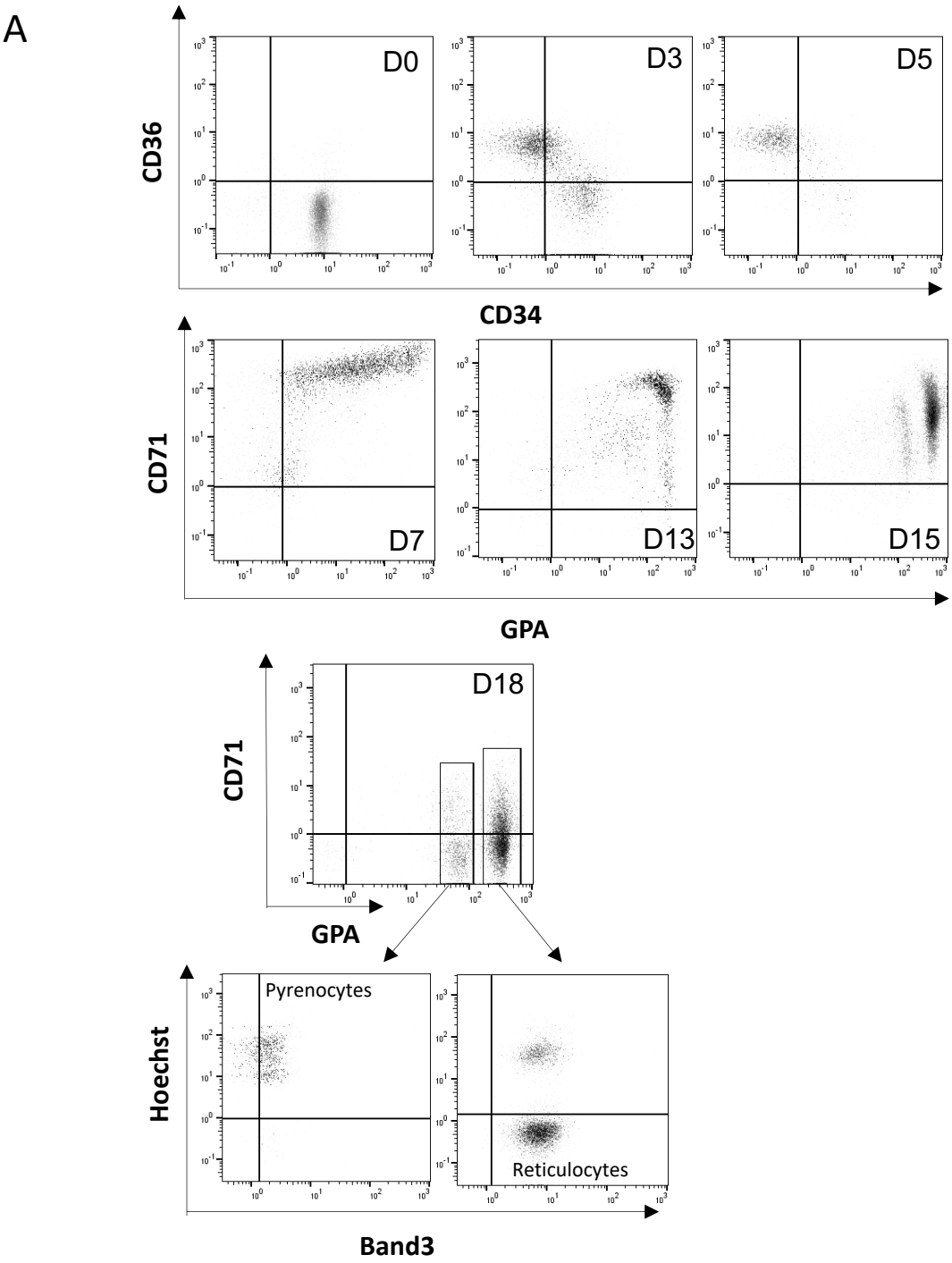

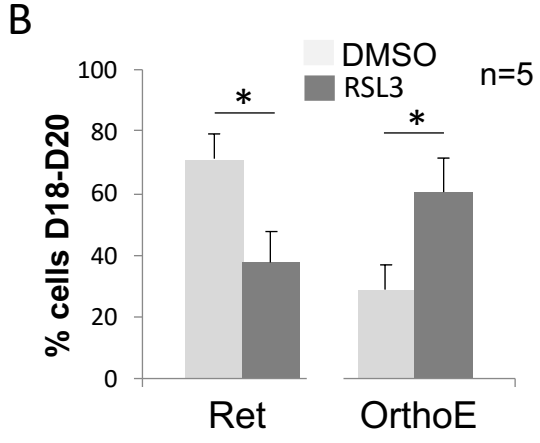

Suppl. Figure 3

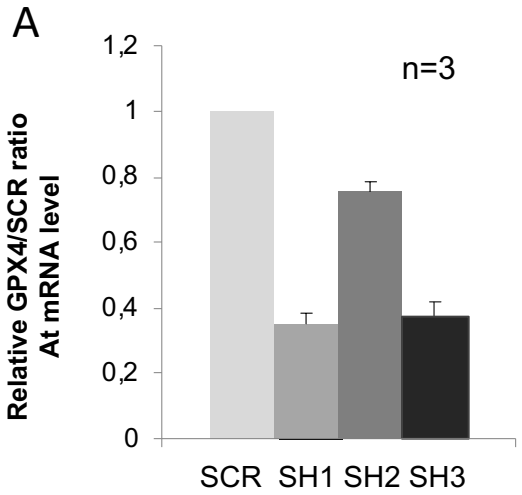

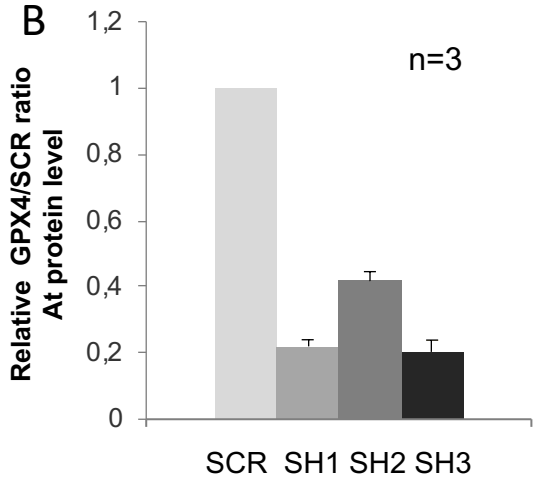

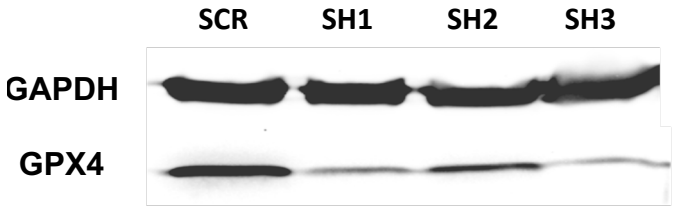

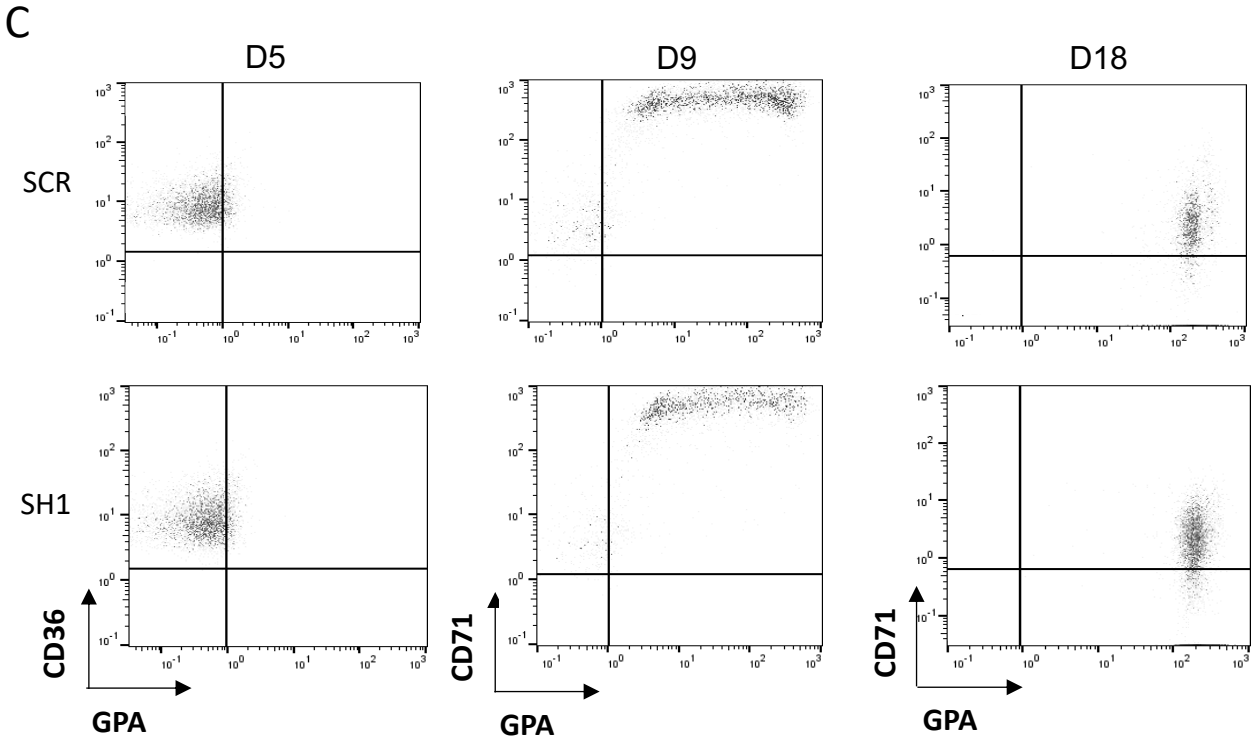

Suppl. Figure 4

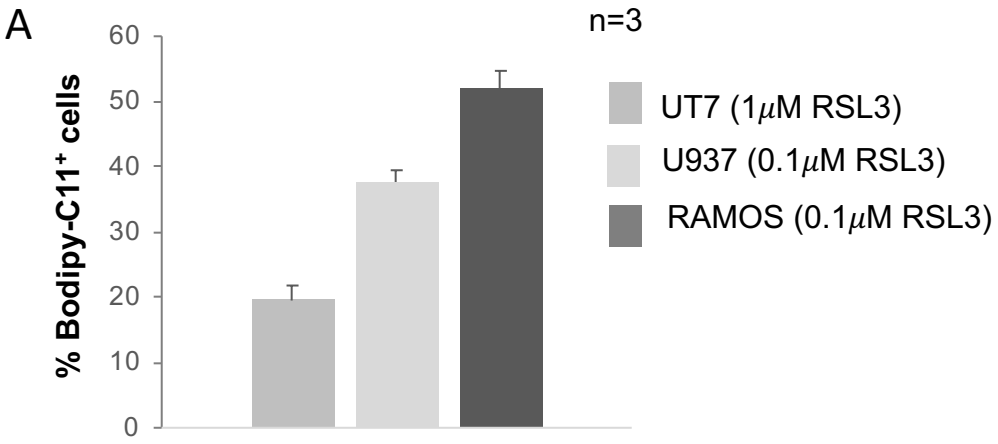

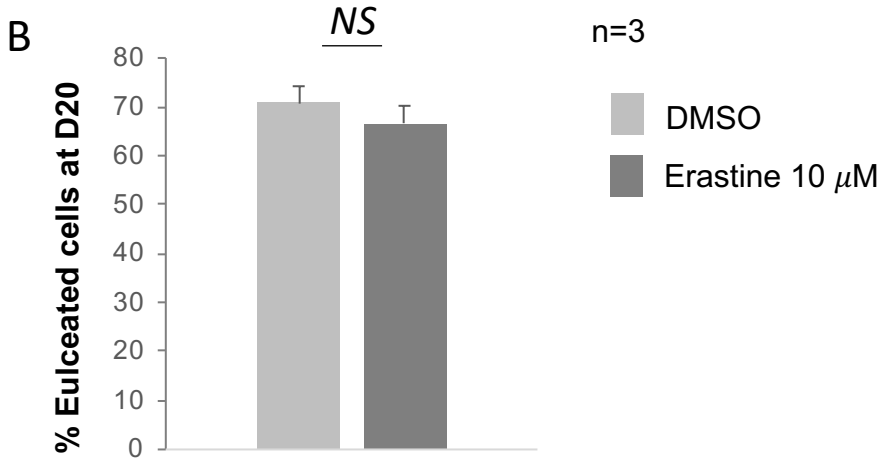

Suppl. Figure 5

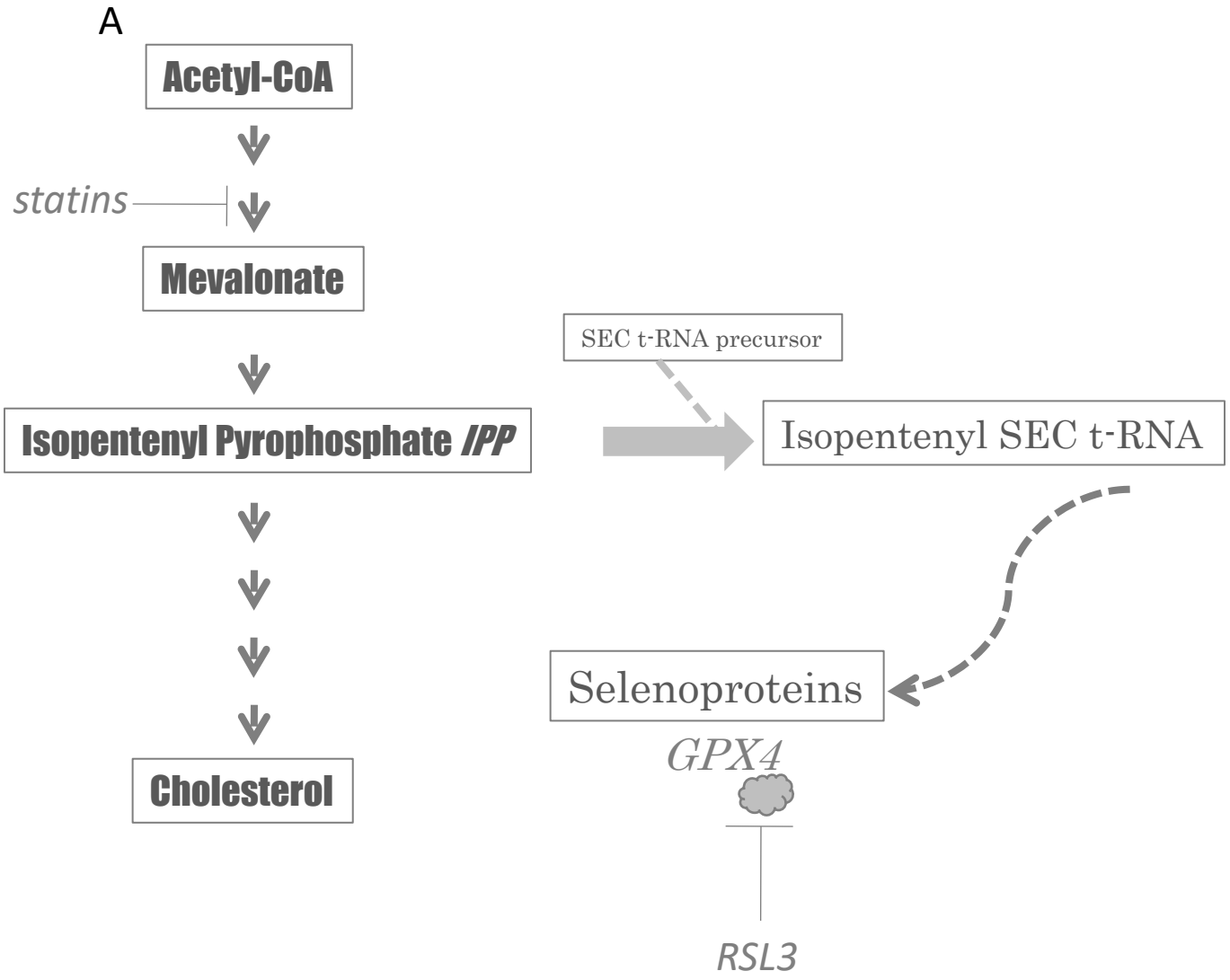

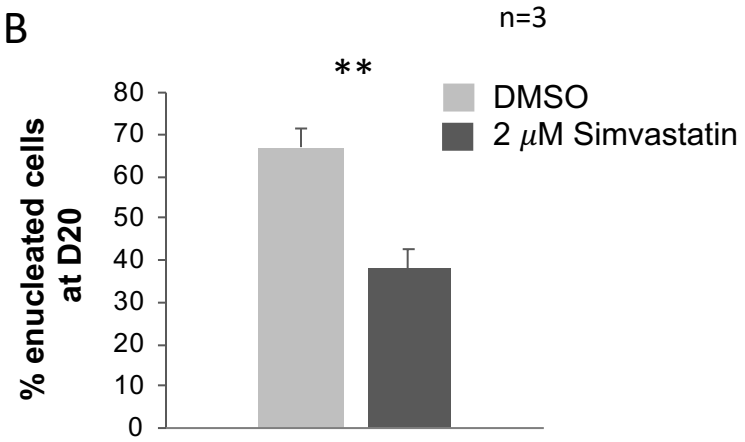

Suppl. Figure 6

A

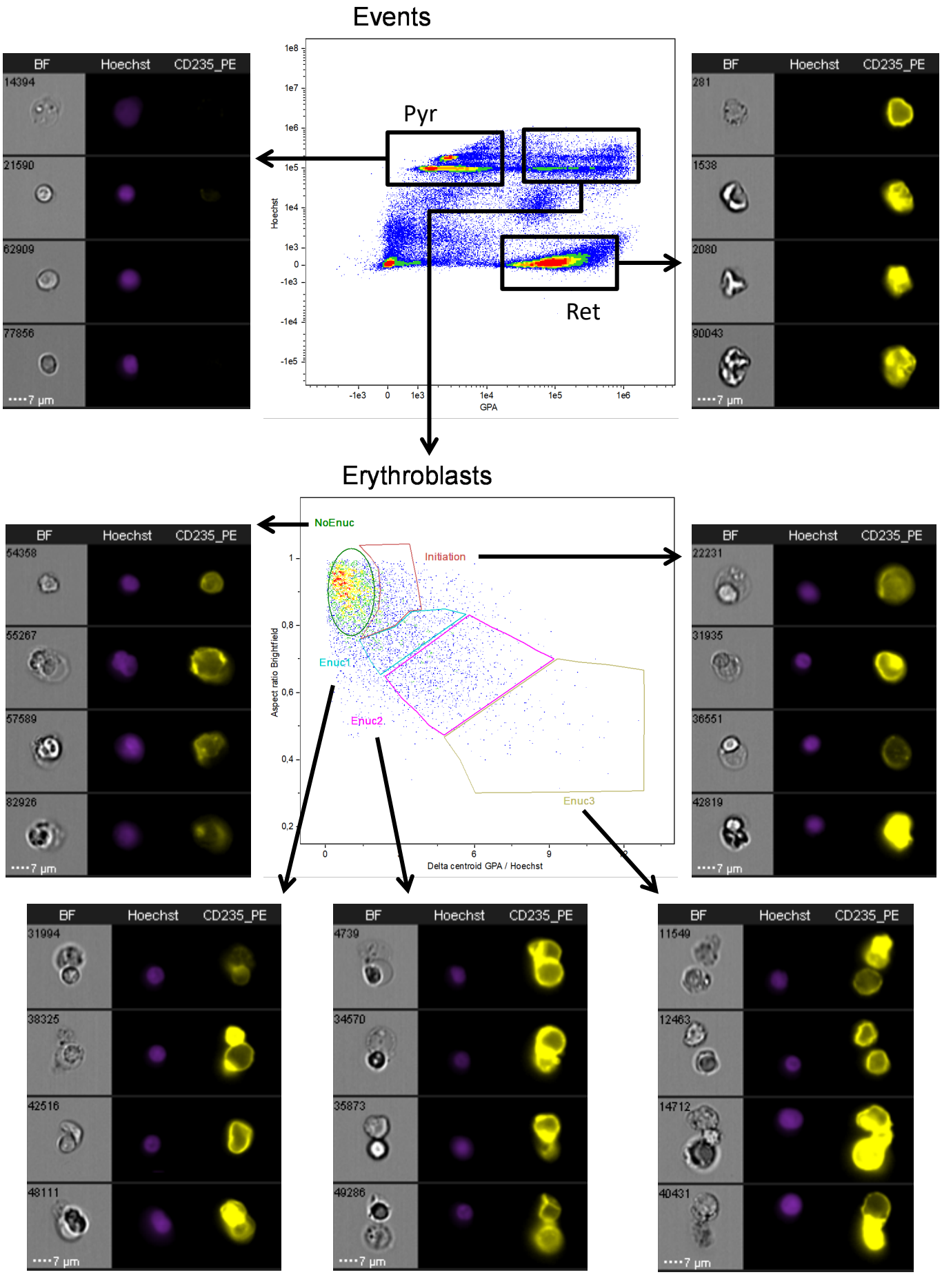

Suppl. Figure 6

B

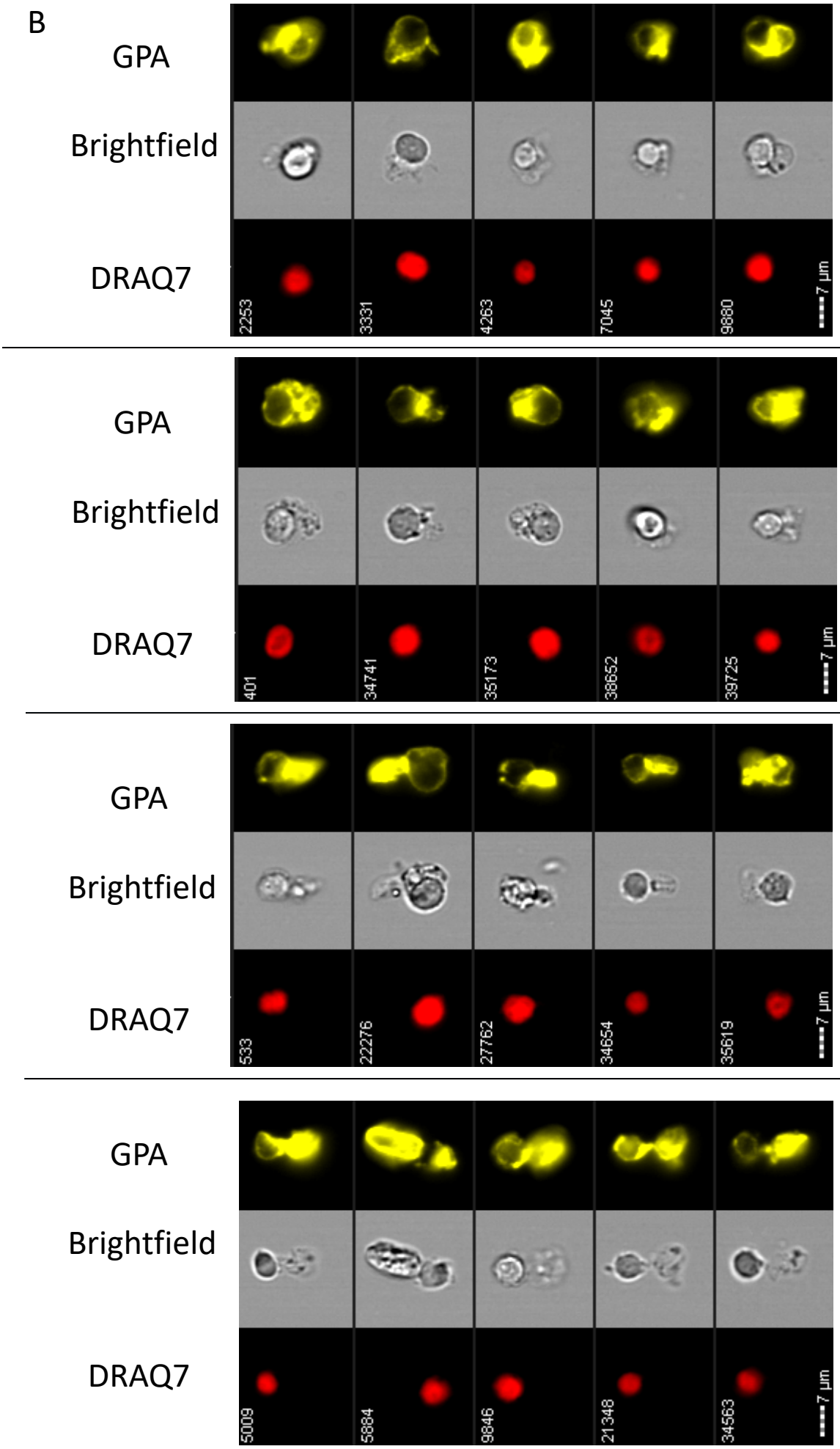

Suppl. Figure 7

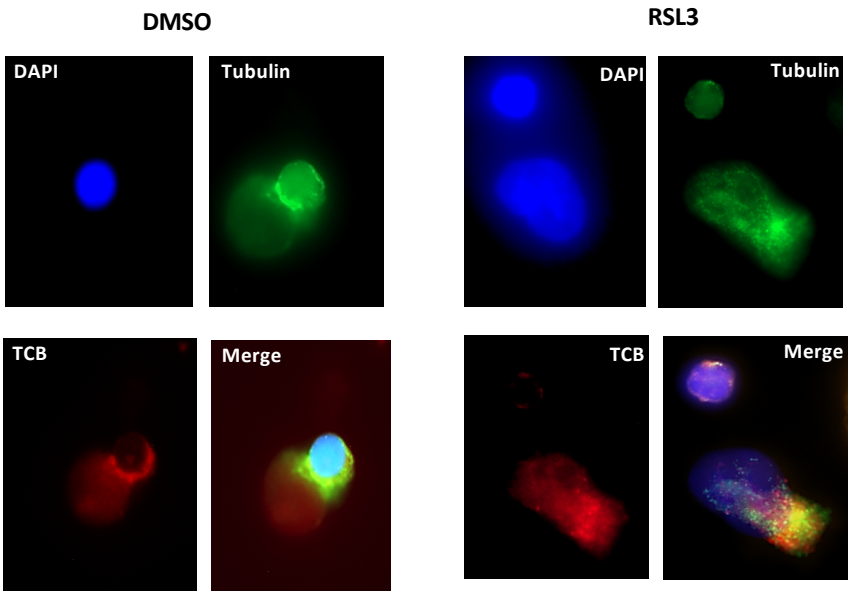

Suppl. Figure 8

A

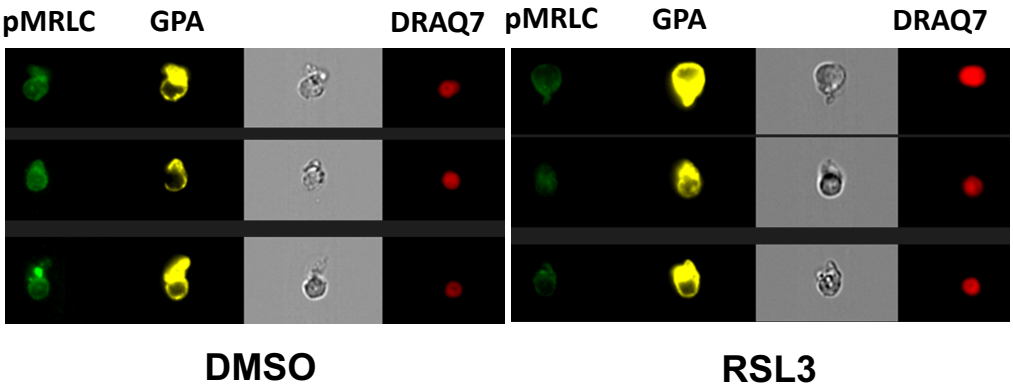

B